

INTRODUCTION TO WAKEFIELDS AND WAKE POTENTIALS*

P. B. WILSON

*Stanford Linear Accelerator Center,
Stanford University, Stanford, California 94309*

TABLE OF CONTENTS

1.	INTRODUCTION	2
2.	BASIC CONCEPTS	2
	2.1 The "Catch-Up" Problem	3
	2.2 Wake Potentials and the Loss Factor	4
	2.3 Wake Potentials and the Loss Factor for a Normal Mode	7
	2.4 Relations Between Wake Potentials and Impedance	9
	2.5 Systems with Cylindrical Symmetry	10
	2.6 Panofsky-Wenzel Theorem	11
3.	METHODS FOR CALCULATING WAKEFIELDS AND WAKE POTENTIALS	12
	3.1 Direct Solution in the Time Domain	12
	3.2 Cylindrical Tube with Weakly Perturbed Walls	14
	3.3 Field Matching	15
	3.4 Wake Potentials for Closed Cavities: The Condon Method	20
	3.5 The Diffraction Model	25
	3.6 Transition Between a Single Cavity and a Periodic Structure	27
4.	SOME APPLICATIONS OF WAKE POTENTIALS	28
	4.1 Single Bunch Beam Loading and Energy Spread	28
	4.2 Single Bunch Transverse Dynamics	31
	4.3 Multiple Bunch Wakefield Effects	33
	4.4 Wakefields from Scrapers and Collimators	34
	4.5 Applications to Storage Rings	36
	ACKNOWLEDGEMENTS	37
	REFERENCES	37

*Work supported by the Department of Energy, contract DE-AC03-76SF00515.

1. INTRODUCTION

What are wakefields and wake potentials, and why are these concepts useful in the physics of linear accelerators and storage rings? We approach this question by first reviewing the basic physical concepts which underlie the mathematical formalism. We then present a summary of the various techniques that have been developed to make detailed calculations of wake potentials. Finally, we give some applications to current problems of interest in accelerator physics. No attempt at completeness can be made in an introductory article of modest length. Rather, we try to give a broad overview and to list key references for more detailed study. It will also be apparent that the last chapter on this subject, with all the loose end neatly tied up, has yet to be written. There are subtle points, there are controversial questions, and active calculations to resolve these questions are continuing at the time of this writing.

In listing references, no attempt has been made to be exhaustive or to present a complete guide to the historical development of each of the topics covered. However, several general references can be recommended to the beginning student of the subject. A. Chao¹ gives an elegant introduction to the basic physics of wake potentials in cylindrically symmetric systems. A general introduction to wake potentials and impedance concepts is given in Ref. 2, Sec. 9. K. Bane et al.³ give the most detailed and complete presentation of the calculation of wake potentials in closed cavities. Finally, K. Bane and M. Sands⁴ review wakefield effects in the diffraction limit for short bunches passing through a cavity with beam tubes, and develop a number of useful analytic expressions for this case.

2. BASIC CONCEPTS

Consider a point charge moving in free space at a velocity close to the velocity of light, c . We know that, viewed in the laboratory frame, the electric and magnetic fields of such a relativistic particle lie nearly in a plane passing through the charge and perpendicular to its path. Thus a second charge moving behind the first charge on the same or on a parallel path, and at the same velocity $v \approx c$, will not be subjected to any forces from the fields produced by the leading charge. The situation is different if the two charges are moving in the vicinity of metallic objects or other boundary discontinuities. The trailing charge still will not experience the direct fields in the wavefront moving with the lead charge. This

wavefront can, however, scatter from the boundary discontinuities, and this scattered radiation will be able to reach the trailing charge and exert forces parallel and perpendicular to its direction of motion. These scattered waves are termed wakefields, and the integrated effects of these wakefields over a given path length of the trailing charge give rise to longitudinal and transverse wake potentials.

If a point charge moves on the axis of a perfectly conducting round pipe at $v \approx c$, the fields in the pipe are identical to the free space fields and hence there are no wakefields. If the particle moves on a trajectory which is parallel to the axis but offset from it, or if the cross section of the pipe is not a circle, the fields in the interior of the pipe are perturbed from their free space values. Even in this case, however, no wakefields are left behind the moving charge. One way to see this is to note that the boundary conditions can still be satisfied without either E_z or B_z field components (we assume the pipe walls and the direction of the particle motion are both parallel to the z axis). The energy flow, in the direction $\vec{E} \times \vec{H}$, is then also in the z direction at every point in the wavefront plane (the plane containing the charge and perpendicular to its path). Thus, there can be no field anywhere behind the wavefront plane. The situation is changed if the pipe is not perfectly conducting. A small E_z field component, related to the dissipation in the pipe walls, is necessarily present on and behind the wavefront plane (see Sec. 3.2).

2.1 The "Catch-Up" Problem

Figure 1 illustrates the wakefields produced by scattering from a small metallic obstacle by the (nearly) plane wavefront of a charge q traveling at $v \approx c$. A test particle traveling a distance s behind the driving charge will not experience the scattered wakefields until it has reached a position z_c , given by

$$z_c \approx \frac{b^2 - s^2}{2s} . \quad (2.1)$$

This "catch-up" distance can be quite large for small s . Taking into account the fact that γ (the usual relativistic factor) is in reality finite, the distance for the scattered radiation to catch up to the exciting charge itself is $z_c \approx \gamma b$.

Figure 2 gives some examples of wakefields excited by a point charge moving past several cylindrically symmetric discontinuities. Figure 2(a) shows a point charge entering and leaving a pipe with thin walls. For $v = c$ the field lines when the charge is in the pipe are the same as in free space, and there is no scattering at the entrance and exit of the pipe. For $v < c$ there will be scattering. In Figs. 2(b)–2(e) the dashed curves are intended only to show the limits of the wakefields, which are contained in a toroidal region with a minor radius which is expanding at velocity c . Exact analytic solutions for the electric and magnetic fields within the toroidal region for these cases have not been obtained for a point

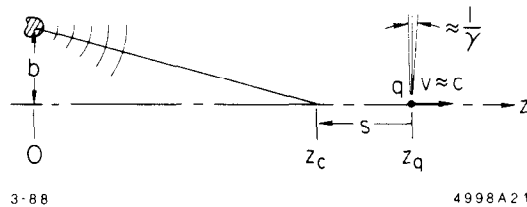


Fig. 1. Figure showing the field of a relativistic charge moving along the z -axis, and the field scattered by a perturbing metallic obstacle.

driving bunch. However, for short bunches computer simulations indicate that the scattered radiation field will be present not only on the expanding wavefront shown by the dashed curves, but will also tend to fill in the entire toroidal volume behind the wavefront. An analytic solution does exist for the case shown in Fig. 2(f), a point charge passing between two parallel conducting planes without beam holes. In this case, discussed in more detail in Sec. 3.4, the fields are confined to the wavefronts shown.

2.2 Wake Potentials and the Loss Factor

The integrated effect of the wakefields of a driving charge on a trailing test particle as both particles pass through a structure, for example the parallel plates of Fig. 2(f), is usually of greater interest than are the details of the wakefields themselves. The integrated fields seen by a test particle traveling on the same or on a parallel path at a constant distance s behind a point charge q are the longitudinal and transverse wake potentials, given by

$$W_z(\vec{r}, \vec{r}', s) = -\frac{1}{q} \int_{z_1}^{z_2} dz [E_z(\vec{r}, z, t)]_{t=(z+s)/c}, \quad (2.2a)$$

$$\vec{W}_\perp(\vec{r}, \vec{r}', s) = \frac{1}{q} \int_{z_1}^{z_2} dz \left[\vec{E}_\perp + c(\hat{z} \times \vec{B}) \right]_{t=(z+s)/c}. \quad (2.2b)$$

Here, \hat{z} is a unit vector in the direction of motion of both the driving and test charges, which are taken to be parallel to the z axis. The transverse offsets of the driving and test charges from the z axis are \vec{r}' and \vec{r} , respectively. In general, the wake potentials are functions of both \vec{r} and \vec{r}' . The driving charge is assumed to enter the cavity structure at $z, t = 0$ and to exit at $z = L$. The test particle enters

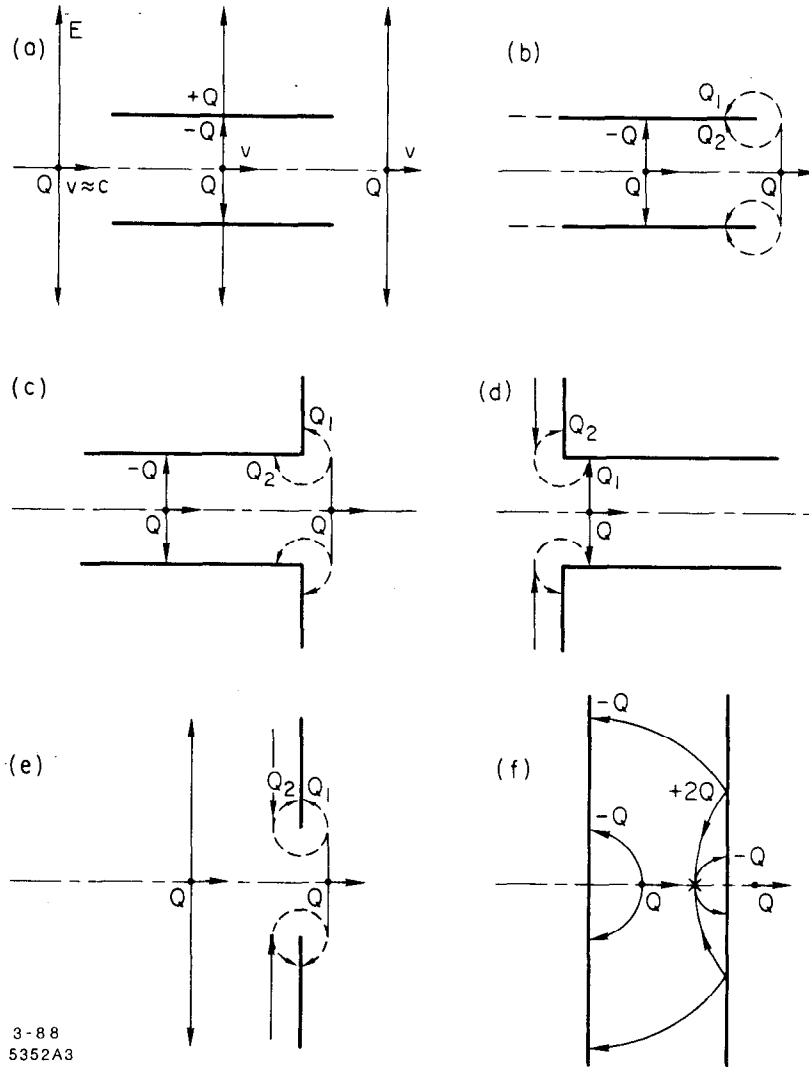


Fig. 2. Wakefields excited by a point charge moving past several cylindrically symmetric discontinuities.

and leaves the cavity at z_1 and z_2 . The longitudinal momentum kick experienced by a test particle of charge e is $\Delta P_z = -(eq/c)W_z(s)$. Note the convention that a positive longitudinal wake is retarding if e and q have the same sign. The transverse momentum kick experienced by the test particle is $\vec{p}_\perp = (eq/c)\vec{W}_\perp(s)$. Note that we assume both driving and test particles are traveling at $v = c$. For $v_e = v_q < c$, the wake potentials will in general be functions of the particle velocity, and the wake potential concept is then much less useful. Also, if the definition in Eqs. (2.2) are to be useful, the driving and trailing charges must be sufficiently relativistic so that their paths through a cavity or structure are not significantly changed from what they would have been in the absence of the induced wakefields.

Once the response to a point driving charge has been calculated, the wake potentials above can be used as Green's functions to compute the potentials in and behind an arbitrary charge distribution. If the line density of the charge distribution is $\lambda(s)$ per unit length, the longitudinal and transverse potentials are

$$V_z(s) = \int_0^{\infty} ds' \lambda(s-s') W_z(s') = \int_{-\infty}^s ds' \lambda(s') W_z(s-s'), \quad (2.3a)$$

$$\vec{V}_{\perp}(s) = \int_0^{\infty} ds' \lambda(s-s') \vec{W}_{\perp}(s') = \int_{-\infty}^s ds' \lambda(s') \vec{W}_{\perp}(s-s'). \quad (2.3b)$$

The potentials in Eqs. (2.3), sometimes called bunch potentials, can be normalized to a charge distribution with unit total charge. These normalized potentials are sometimes also called wake potentials. This can be a source of confusion, but it is usually clear from the context whether we are referring to the impulse (or delta function) wake potential due to a point driving charge, or to the net wake potential within and behind a charge distribution.

Once the longitudinal bunch potential is known, the total energy loss to the wakefields is given by

$$\Delta U = \int_{-\infty}^{\infty} ds \lambda(s) V_z(s) = \int_{-\infty}^{\infty} d\tau I(\tau) V_z(\tau), \quad (2.4a)$$

where $\tau = s/c = t - z/c$ and $I(\tau) = c\lambda(s)$ is the current flow in the charge distribution. Equations (2.3) can of course also be written in terms of $I(\tau)$ in place of $\lambda(s)$. A useful quantity, the loss factor, is now defined as

$$k_{\ell} = \frac{\Delta U}{q^2}. \quad (2.4b)$$

An analogous transverse quantity, the transverse impulse factor, is defined by

$$\vec{k}_{\perp} \equiv \frac{1}{q^2} \int_{-\infty}^{\infty} ds \lambda(s) \vec{V}_{\perp}(s). \quad (2.5)$$

The total momentum kick experienced by the charge distribution is then $\vec{p}_{\perp} = q^2 \vec{k}_{\perp}/c$.

By substituting Eq. (2.3a) in Eqs. (2.4a), we can prove a useful theorem concerning the longitudinal wakefield for a point charge or for a very short charge

distribution. Assume the bunch or distribution $\lambda(s)$ is so short that the delta function wake potential can be treated as a constant on the scale of the bunch length, $W_z(s) = W_z(0^+)$, where 0^+ is a small positive distance. An integration by parts then gives

$$\Delta U = \frac{1}{2} q^2 W_z(0^+) . \quad (2.6a)$$

By definition the energy loss for a point bunch is related to the effective wake potential acting on the bunch by

$$\Delta U = qV(0) = q^2 W_z(0) = q^2 k_\delta , \quad (2.6b)$$

where k_δ is the loss factor for a point bunch. Thus we can say that the wake potential immediately behind a point charge is twice the effective wake “seen” by the charge itself:

$$W_z(0^+) = 2W_\delta(0) . \quad (2.6c)$$

This has been called the fundamental theorem of beam loading.² By causality $W_\delta(0^-)$ is, of course, zero.

2.3 Wake Potentials and the Loss Factor for a Normal Mode

If we consider a point charge interacting in a cavity with a single mode having resonant frequency ω_n , then it is reasonable to expect that along a path behind a driving point charge the induced potential will have the form

$$V_{zn}(s) = -\hat{V}_n \cos \frac{\omega_n s}{c} . \quad (2.7a)$$

In other words, the wake is maximum retarding just behind the driving charge, and it rings at the mode frequency ω_n . A more precise justification for this expression will be given in Sec. (3.4). From Eqs. (2.6), the peak value of the induced potential must then be

$$\hat{V}_n = q W_z(0^+) = 2qk_{\delta n} , \quad (2.7b)$$

and the longitudinal wake potential is

$$W_{zn}(s) = -\frac{V_{zn}(s)}{q} = 2k_{\delta n} \cos \left(\frac{\omega_n s}{c} \right) , \quad s > 0 . \quad (2.7c)$$

Combining Eq. (2.7b) with $k_{\delta n} \equiv U_n/q^2$, where $U_n = (\Delta U)_n$,

$$k_{\delta n} = \frac{\hat{V}_n^2}{4U_n} . \quad (2.8)$$

Note that $e\hat{V}_n$ can be interpreted as the peak energy gain from the field induced in the n^{th} mode for a relativistic particle which crosses the cavity after the driving

charge has exited, leaving behind energy U_n . This energy could as well have been produced by any source, for example an external rf generator. Thus, $k_{\delta n}$ as defined above is a property of the charge-free cavity geometry, and as such can be calculated using computer programs which solve the homogeneous Maxwell's equations. However, we will find later that the wake potential described by Eq. (2.7c) is valid even if the driving and test charges are both in the cavity at the same time, as long as the two particles follow the same path through the cavity.

If the cavity or structure is excited by a gaussian bunch with rms length σ , the induced potential can be obtained by substituting Eq. (2.7c) into Eq. (2.3a) to give

$$V_{zn}(s) = \frac{-2qk_{\delta n}}{\sqrt{2\pi}\sigma} \int_{-\infty}^s ds' \cos \left[\frac{\omega_n(s-s')}{c} \right] \exp \left(-\frac{s'^2}{2\sigma^2} \right) . \quad (2.10a)$$

If position s is at least several bunch lengths behind the center of the bunch, the upper limit in the above integration can be taken as infinity to give

$$V_{zn}(s) = -2qk_{\delta n} \cos \left(\frac{\omega_n s}{c} \right) \exp \left(-\frac{\omega_n^2 \sigma^2}{2c^2} \right) , \quad (2.10b)$$

$s \gtrsim 3\sigma .$

Substituting Eq. (2.10a) in Eqs. (2.4) and integrating by parts, we obtain the total loss factor for a gaussian bunch interacting with the n^{th} normal mode,

$$k_{\ell n}(\sigma) = k_{\delta n} \exp \left(-\frac{\omega_n^2 \sigma^2}{c^2} \right) . \quad (2.10c)$$

In analogy to Eq. (2.7c), under certain restricted conditions the longitudinal dependence of the deflection wake can also be factored out (see Sec. 3.4) to give

$$\vec{W}_{\perp n}(s) = 2k_{\perp n} f(\vec{r}, \vec{r}') \sin \left(\frac{\omega_n s}{c} \right) , \quad (2.11)$$

where $k_{\perp n}$ is again a parameter for the n^{th} mode which depends only on the geometry of the charge-free cavity or structure. In particular, Eq. (2.11) holds for the important case of the deflection wake in the beam tube region of an infinite periodic structure. Thus, for this case the transverse wake is a sum of sine-like modes which vanish at the position of the driving charge, i.e., a point charge cannot deflect itself. This is in contrast to the cosine-like longitudinal modes, which must always produce a retarding potential at the driving charge itself.

2.4 Relations Between Wake Potentials and Impedance

In Sec. 3 we will find that the boundary value problem for the charge-driven fields in a structure is sometimes easier to solve in the frequency domain rather than directly in the time domain. Time and frequency domain quantities are then related by the Fourier transform. For example, the impedance in the frequency domain is obtained from the time domain wake potential by

$$Z(\omega) = \int_0^{\infty} W_z(\tau) \exp\{-i\omega\tau\} d\tau \equiv \widetilde{W}_z(\tau), \quad (2.12a)$$

$$Z(k) = \int_0^{\infty} W_z(s) \exp\{-iks\} ds \equiv \widetilde{W}_z(s) = c[Z(\omega)]_{\omega=kc} \quad (2.12b)$$

where $k = \omega/c$, $s = c\tau = ct - z$, and the lower limit of integration is zero since $W_z(s) \equiv 0$ for $s < 0$. Similarly,

$$\begin{aligned} I(\omega) &= \widetilde{I}(\tau) \quad ; \quad \lambda(k) \equiv \widetilde{\lambda}(s) = [I(\omega)]_{\omega=kc} \\ V(\omega) &= \widetilde{V}(\tau) \quad ; \quad V(k) \equiv \widetilde{V}(s) = c[V(\omega)]_{\omega=kc} \end{aligned}$$

In these transforms the lower limit of integration must of course be $-\infty$.

From Eq. (2.3a) we know that $V(\tau)$ is the convolution of the delta-function wake, $W_z(\tau)$, and the current distribution, $I(\tau)$. The convolution theorem⁵ of Fourier transform theory tells us that the transform of the convolution of two functions is the product of their individual transforms. Thus,

$$V(\omega) = I(\omega) Z(\omega), \quad (2.13a)$$

$$V(k) = \lambda(k) Z(k). \quad (2.13b)$$

These results can also be easily proven directly, for example by substituting Eq. (2.3a) in the definition of the transform and reversing the order of integration to obtain Eq. (2.13a). If the impedance is known, for example from a frequency domain calculation, then the delta function wake potential is calculated from the inverse transform as

$$W_z(s) = \frac{1}{2\pi} \int_{-\infty}^{\infty} Z(\omega) \exp(i\omega s/c) d\omega = \frac{2}{\pi} \int_0^{\infty} Z_R(\omega) \cos\left(\frac{\omega s}{c}\right) d\omega. \quad (2.14)$$

To obtain this result, we depend on the fact that the wake potential is both real and causal, that is $W_z(s) \equiv 0$ for $s < 0$. If $W_z(s)$ is to be real, then $Z_R(\omega)$ and

$Z_I(\omega)$ must be even and odd functions of frequency respectively, and the lower limit of integration can be changed from $-\infty$ to 0. If $W_z(s)$ is to be causal, then $Z_R(\omega)$ and $Z_I(\omega)$ are related by the Hilbert transform, and this introduces a second factor of two (see Ref. 2, Sec. 9.3, for a more detailed development).

From the power theorem of Fourier transform theory⁵ (the asterisk indicating complex conjugate),

$$\Delta U = \int_{-\infty}^{\infty} V(t) I(t) dt = \frac{1}{2\pi} \int_{-\infty}^{\infty} V(\omega) I^*(\omega) d\omega .$$

Using Eq. (2.13a) and the symmetry properties of the impedance function,

$$k_\ell = \frac{\Delta U}{q^2} = \frac{1}{\pi q^2} \int_0^{\infty} Z_R(\omega) I^2(\omega) d\omega . \quad (2.15a)$$

For a gaussian bunch, $I(\omega) = q \exp(-\omega^2 \sigma^2 / 2c^2)$ and

$$k_\ell = \frac{1}{\pi} \int_0^{\infty} Z_R(\omega) \exp\left(-\frac{\omega^2 \sigma^2}{c^2}\right) d\omega . \quad (2.15b)$$

For a high Q resonant mode,

$$Z_R(\omega) = \frac{Z_0}{1 + [2Q(\omega - \omega_0)/\omega_0]^2} .$$

The integration in Eq. (2.15b) then gives, together with Eq. (2.10c),

$$k_{\delta n} = \frac{\omega_n}{2} \left(\frac{Z_0}{Q} \right)_n . \quad (2.16)$$

Note that $Z_0 = R/2$, where R is the usual accelerator definition of the shunt impedance.

2.5 Systems with Cylindrical Symmetry

Most accelerating structures for linacs and storage rings are cylindrically symmetric. The longitudinal and transverse wake potentials can in this case be expanded in terms of multipoles having an azimuthal variation proportional to $\cos m\theta$, where $m = 0$ gives the azimuthally symmetric (monopole) potential, $m = 1$ the dipole potential, etc. We make the assumptions that the driving charge is moving parallel to the axis of symmetry of the structure, that all quantities depend on z and t only as functions of $s = ct - z$, and that all forces are

averaged over one period in the case of an infinite periodic structure. Then it can be shown^{6,7} that

$$W_z^{(m)} = r_0^m r^m F'(s) \cos m\theta, \quad (2.17a)$$

$$\vec{W}_\perp^{(m)} = mr_0^m r^{m-1} F(s) \left[\hat{r} \cos m\theta - \hat{\theta} \sin m\theta \right]. \quad (2.17b)$$

Here, \vec{r}_0 is the transverse offset of the driving charge from the structure axis. It is assumed to be at $\theta = 0$. The field point (location of the test charge) is at radius \vec{r} , and $F'(s) = dF/ds$ for $m \neq 0$. For $m = 0$, $\vec{W}_\perp \equiv 0$ and $F'(s) = F_0(s)$. Both wake potentials vanish, of course, for $s < 0$. The important thing to note is that the dependence on longitudinal and radial variables is separable for both of the wake potentials. The simple scaling with radius allows the wake potentials to be calculated at the radius of the beam hole, thus avoiding the catch-up problem inherent in an integration along or near the axis. This will be discussed more fully in Sec. 3.1. Note that for $m = 0$ the longitudinal wake is independent of radial position in the beam hole region. For the dipole mode the transverse kick is uniform over the beam hole region and is in the direction of offset of the driving charge. This is seen more clearly by rewriting Eq. (2.17b) as

$$\vec{W}_\perp^{(1)} = \vec{r}_0 F(s). \quad (2.18)$$

In the derivation of Eqs. (2.17), it was assumed that the wake potentials are averaged over one period in the case of an infinite periodic structure, or are calculated for a single cavity with input and output beam tubes of equal radius. If there is metal between the beam and the axis of symmetry, as for example in a coaxial cavity, there are additional terms⁶ in the wake potentials. In the case of the longitudinal wake, for example, there is a term proportional to $\ln(r)$ for $m = 0$, and to r^{-m} for $m > 0$.

2.6 Panofsky-Wenzel Theorem

Panofsky and Wenzel⁸ proved a theorem concerning the net transverse kick experienced by test charge crossing a closed cavity of arbitrary shape containing electromagnetic fields derived from a vector potential \vec{A} only (no free charges):

$$\vec{p}_\perp = e \int_0^L dz \left[\vec{\nabla}_\perp A_z(z, t) \right]_{t=z/c} = \frac{ie}{\omega_0} \int_0^L dz \left[\vec{\nabla}_\perp E_z(z, t) \right]_{t=z/c}. \quad (2.19)$$

In deriving these expressions it is assumed that \vec{A}_\perp vanishes at $z = 0 = L$, i.e., either the path of the test charge begins and ends in a field free region (as in beam

tubes), or the cavity end walls are normal to the path. Even if this is not the case, the small additional boundary term can usually be neglected. The second expression in Eq. (2.19) assumes a single mode ringing as $e^{i\omega_0 t}$. These expressions hold whatever the source of the cavity fields, which could be an external rf generator or a driving charge which has passed through the cavity earlier. If we assume that such a driving charge has already left the cavity and look at distance $s = ct - z$ behind the charge, then for $s > L$ Eq. (2.19) gives

$$\frac{\partial \vec{W}_\perp}{\partial s} = \frac{c}{eq} \frac{\partial \vec{p}_\perp}{\partial s} = -\frac{1}{q} \int_0^L dz \left[\vec{\nabla}_\perp E_z(z, t) \right]_{t=(s+z)/c} = \vec{\nabla}_\perp W_z. \quad (2.20)$$

In the literature on wake potentials, it is this relation between the longitudinal derivative of the transverse wake potential and the transverse gradient of the longitudinal potential that is referred to as the Panofsky–Wenzel theorem. Note that in the previous section, the wake potentials given in Eqs. (2.17) for cylindrically symmetric structures obey this theorem for any value of s . However, from the derivation of the theorem it also holds for a closed cavity of arbitrary shape for $s > L$. It will be shown in Sec. 3.4 that the theorem also holds for $0 < s < L$ in a structure of arbitrary cross section with translational symmetry and with end planes normal to the path of the particles, and also for a closed cavity of arbitrary shape if the driving and test particles follow the same path.

3. METHODS FOR CALCULATING WAKEFIELDS AND WAKE POTENTIALS

3.1. Direct Solution in the Time Domain

The most straightforward way to compute wakefields is to solve Maxwell's equations directly in the time domain. For all but the simplest boundary conditions, however, this must be done numerically. By discretizing Maxwell's equations on a mesh, T. Weiland^{9,10} has developed a useful code, TBCI, for calculating the fields induced by a bunch interacting with any cylindrically symmetric structure. As an example of a TBCI output, Fig. 3 shows the wakefields induced by a gaussian bunch passing through a typical cavity for a storage ring rf system. The wake potential could in principle be calculated by integrating the wakefield along the path of the test particle (for example along the axis) using Eqs. (2.2). However, the catch-up problem discussed in Sec. 2.1 poses a difficulty. If, for example, we want to know the wake potential 1 mm behind the leading edge of a bunch traveling through a structure with a 5 cm radius beam aperture, (typical for a storage ring cavity), then Eq. (2.1) implies that the integration must be carried forward along the axis in the downstream beam tube for at least 125 cm beyond the end of the structure. This can lead to an unacceptable increase in the computation time. However, as discussed in Sec. 2.5, in the case of a cylindrically symmetric

structure with input and output beam tubes of equal radius, the wake potentials scale with radius in a simple way. This allows the integration for the longitudinal wake of a cavity to be carried out at the beam tube radius, where E_z vanishes except across the cavity gap itself. The longitudinal wake potential can then be scaled to any radius using Eq. (2.17a). The situation is similar for the transverse wake, but less obvious. From Eq. (2.17b) the dipole wake is in the θ direction at $\theta = 90^\circ$. A transverse kick in the θ direction must come from the E_θ or B_r field component, both of which vanish at the metal walls at radius $r = a$ in the beam tube region. The transverse wake can therefore be obtained by integrating the azimuthal component over the cavity gap at $r = a$ and $\theta = 90^\circ$.

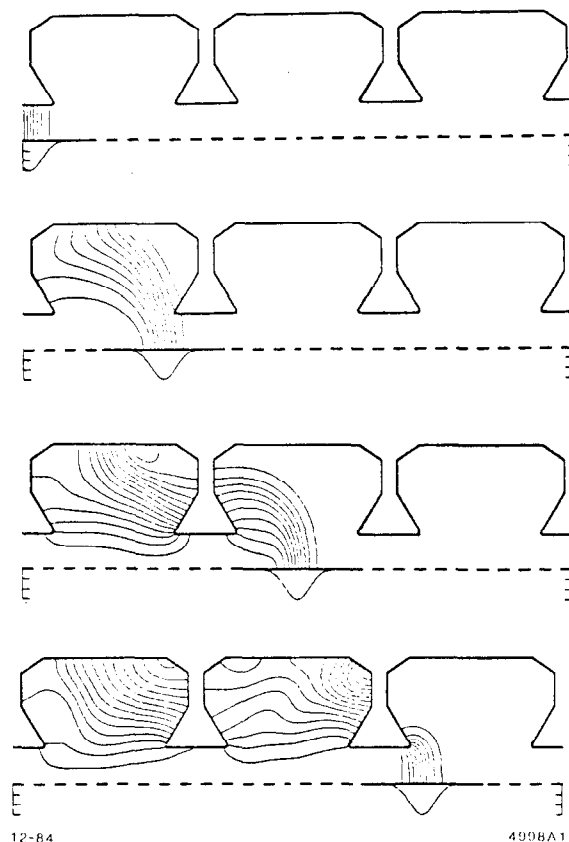


Fig. 3. Electric wakefield produced by a gaussian bunch traversing a PETRA cavity.¹⁰

Weiland's code TBCI, which solves Maxwell's equations on a rectangular mesh, has been singled out for special mention here since it is widely available and in current use at most accelerator laboratories. Similar codes have, however, been written by others. T. Shintake¹¹ solves the inhomogeneous wave equation for the

vector potential on a rectangular mesh, and A. Novokhatsky¹² solves for fields on a mesh of irregular quadrilaterals. More recently, a fully three dimensional version of TBCI, the MAFIA code T3, has been developed by Weiland and his coworkers.¹³

3.2 Cylindrical Tube with Weakly Perturbed Walls

As mentioned previously, a charge traveling parallel to the axis of a perfectly conducting cylindrical tube generates no wakefields. However, even a small perturbation in the boundary condition at the wall changes this picture. Perhaps the simplest perturbation is to allow the wall to become slightly resistive. The problem of the longitudinal and transverse wakefields in a slightly resistive pipe of circular cross section has been investigated in a classic paper by Morton, Neil and Sessler.¹⁴ An elegant tutorial exposition of this problem is given by Chao.¹⁵ The delta-function wake potentials per unit length for this case are

$$m = 0 : W_z(s) = -\frac{c}{2\pi b} \left(\frac{Z_0}{\pi\sigma_c} \right)^{1/2} s^{-3/2}, \quad (3.1a)$$

$$m = 1 : \vec{W}_\perp(s) = \frac{\vec{r}_0 c}{\pi b^3} \left(\frac{Z_0}{\pi\sigma_c} \right)^{1/2} s^{-1/2}, \quad (3.1b)$$

where b is the pipe radius, \vec{r}_0 the offset of the unit driving charge from the axis, Z_0 the impedance of free space and σ_c the conductivity. Recall that a negative longitudinal wake is, by the definition in Eq. (1.2a), accelerating. Thus, the wake appears to be accelerating for all values of s . However, in deriving the above expressions, it was assumed that s is greater than a critical distance s_0 given by

$$s_0 = \left(\frac{b^2}{Z_0\sigma_c} \right)^{1/3}. \quad (3.2)$$

It can be shown¹⁵ that at $s \approx s_0$ the sign of the longitudinal wake changes from accelerating to retarding. At the position of the driving charge itself, the retarding field is just that required to give an energy loss which exactly balances the heat generated in the wall. The longitudinal field immediately behind a driving point charge in the limit $s \ll s_0$ is shown¹⁵ to be just twice the retarding field experienced by the charge itself, in agreement with the so-called fundamental theorem of beam loading mentioned in Sec. 2.2. It is worth noting that this theorem can also be proved for normal modes in a cavity or structure using conservation of energy.¹⁶

The impulse wakes in Eqs. (3.1) can now be used to find the potentials in a gaussian bunch. Some useful results are given in Ref. 3, Sec. 3.2. In Ref. 3, Sec. 3.1, the longitudinal wake potential for a line charge traveling parallel to the surface of a resistive slab is also derived.

The longitudinal and transverse wake potentials for a cylindrically symmetric structure with a radius $a(z) = a_0[1 + \epsilon s(z)]$, where $s(z)$ is a periodic function of z and ϵ is a perturbation parameter, have been considered by several authors. This boundary value problem is more readily attacked by working with the Fourier transforms of the field components (we should note that this was also the case in calculating the fields for a point charge moving in a pipe with resistive walls). Using this technique for a cylindrical pipe with a weakly perturbed wall geometry, Chatard-Moulin and Papiernik^{17,18} have calculated the longitudinal wakefield and the loss factor k_ℓ for a gaussian bunch as a function of γ and σ_z for the case $s(z) = \cos^8(\pi z/p)$. It is interesting to note that for large γ the loss factor diverges approximately as σ_z^{-1} for small bunch lengths. Cooper, Krinsky and Morton¹⁹ compute the transverse wake potential in and behind a gaussian bunch using a similar perturbation method.

A bellows is also an example of a cylindrical pipe with a weakly corrugated wall. The longitudinal and transverse wake potentials for a bellows are important for beam stability calculations in circular machines. One problem with the perturbation approach used in Refs. 17-19 is that it breaks down if the slope of the wall with respect to the axis is vertical at any point, which is often the case in a practical bellows. Calculations by Kheifets and Zotter,²⁰ and by Krinsky and Gluckstern,²¹ get around this difficulty. However, in these calculations the longitudinal and transverse impedances are obtained only in the low frequency range. Thus the method is not well suited to obtaining the short-range wake potentials.

3.3 Field Matching

The simple cylindrically symmetric structure shown in Fig. 4(a), in which all surfaces are parallel or perpendicular to the axis, can serve as a rough model for many accelerating structures and rf cavities. The four parameters a , b , g and p specify the disk hole radius, the cavity radius, the cavity length and the periodic length, respectively. If p is long compared to g , the model approaches a chain of isolated pillbox cavities with beam tubes, as shown in Fig. (4b).

A field matching technique can be applied to the structure of Fig. (4a) to solve for the traveling wave field components which are synchronous with a relativistic charge moving in the beam tube region $r < a$. In this region traveling wave fields which are functions of $kz - \omega t$ are assumed, while standing wave fields are assumed in the cavity region, $b > r > a$. The tangential field components are matched across the boundary shown by the dashed line at radius $r = a$ shown in Fig. (4a). A match is possible only at certain specific values of frequency, the eigenfrequencies of the problem. The field components can be either the time domain fields or their Fourier transforms. Using a matching of the time domain field components, E. Keil²² developed the code KN7C, which calculates the frequencies for the source-free monopole ($m = 0$) modes which have phase velocities equal to c . The loss parameter per unit length, $k_n = E_{zn}/4u_n$ where

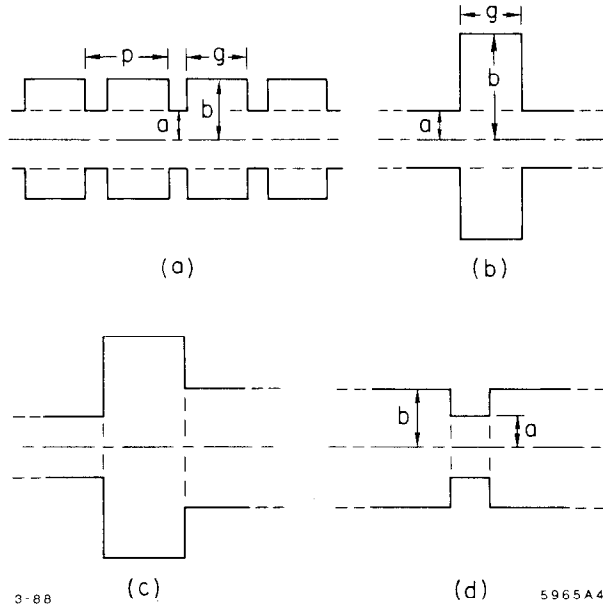


Fig. 4. Examples of cylindrically symmetric structures with jumps in cross section.

E_{zn} is the axial synchronous field component and u_n is the stored energy per unit length for the n^{th} mode, can also be obtained from information in the output of the program. From Eq. (2.7c) the longitudinal wake potential for the first N modes is

$$W_z(s) = \sum_{n=1}^N 2k_n \cos\left(\frac{\omega_n s}{c}\right). \quad (3.3)$$

It is worthwhile to emphasize again that the k_n 's in the expression have been calculated by solving the source-free Maxwell's equations, but that Eq. (3.3) is valid for the charge-driven modes since the structure is both periodic and cylindrically symmetric (see Sec. 2.5).

Because of limitations set by computer time and numerical accuracy, the number of modes that can reasonably be calculated is typically on the order of a few hundred. This corresponds to an upper mode frequency of about thirty times the fundamental (lowest frequency) mode. The wake potential is therefore known to a distance given approximately by $c/\omega = \lambda_0/60\pi$, where λ_0 is the fundamental mode wavelength. This is about 0.5 mm for the SLAC wavelength of 105 mm. The short range longitudinal wake for 450 modes for the SLAC disk loaded structure is shown by the dashed line in Fig. 5. This wake is inadequate to serve as a Green's function for calculating the bunch potential for bunch lengths less than one millimeter or so. (At SLAC, bunch lengths of interest fall in the range 0.25 to 1.5

mm.) The situation is resolved by adding a so called “analytic extension” to the wake potential obtained by summing modes. The functional form of the analytic extension will depend on the model chosen for the impedance in the high frequency limit. The proper model to be used for a gaussian bunch in a periodic structure depends on the number of cells and on the bunch length. This question will be discussed in more detail in Sec. (3.5). A model which describes the impedance for many practical structures of interest is the so-called optical resonator model. The history and details of this model are given in Ref. 23. The correction to the longitudinal wake potential can be written, in analogy with Eq. (3.3),

$$\Delta W_z(s) = 2 \int_{\omega_N}^{\infty} \frac{dk(\omega)}{d\omega} \cos\left(\frac{\omega_n s}{c}\right) d\omega. \quad (3.4a)$$

By comparison with Eq. (2.14), we have

$$\pi \frac{dk}{d\omega} = Z_R(\omega) = A\omega^{-3/2}. \quad (3.4b)$$

We have assumed the validity of the optical resonator model, which predicts $Z_R(\omega) \sim \omega^{-3/2}$ for ω_N is sufficiently high. Equation (3.4) can now be integrated to give

$$\Delta W_z(s) = \frac{4A}{\pi\omega_N^{1/2}} \left\{ \cos x - \sqrt{\frac{\pi x}{2}} \left[1 - 2S\left(\sqrt{\frac{2x}{\pi}}\right) \right] \right\}_{x=\omega_N s/c}, \quad (3.5)$$

where S is the Fresnel integral and $A = Z_R(\omega_N) \omega_N^{3/2}$. Although the constant A is specified analytically by the optical resonator modal, it is often treated in practice as an adjustable constant, obtained by fitting the binned values of Δk from the modal sum plotted on a log-log scale versus increments $\Delta\omega$ in frequency (see Ref. 24). The amount of the added wake is then found to be just that needed to compensate for the ringing in the modal sum wake, caused by truncating the sum at ω_N . The result is a smooth short-range total wake, as shown by the solid curve in Fig. 5. The dot-dash curve shows the wake for the fundamental (accelerating) mode. This wake is important in beam loading calculations.

A time domain field matching code (TRANSVRS) for the $m > 0$ modes has been developed by Bane and Zotter²⁵ for the four parameter structure of Fig. 4(a). Again, the program solves for the frequencies $\omega_n^{(m)}$ of the traveling wave modes with symmetry $\cos m\theta$ which have a space harmonic component which is synchronous with a velocity of light particle. For each synchronous mode, the program solves for the field components and stored energy per unit length. In the

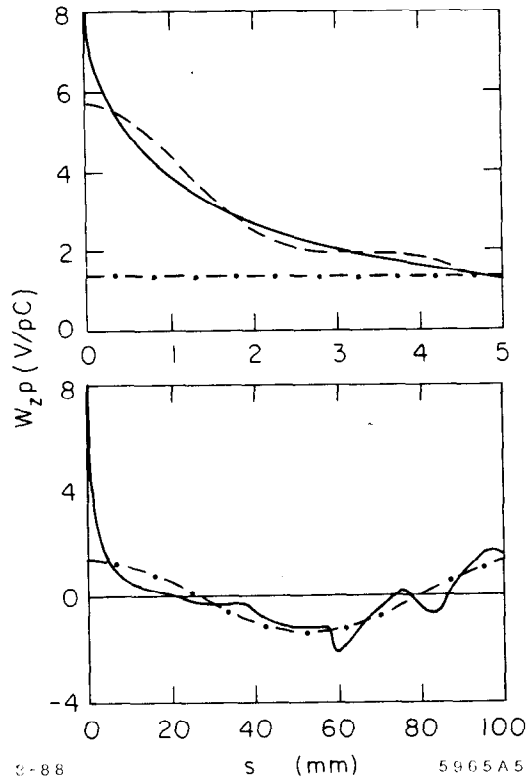


Fig. 5. Short range longitudinal ($m = 0$) wake for the SLAC structure ($a = 1.165$ cm, $b = 4.13$ cm, $d = 3.50$ cm, $g = 2.92$ cm). Dashed curve shows the sum of 450 modes, dot-dash curve the fundamental accelerating mode only.

following section we show that the dipole wake for a unit driving charge which is offset by distance r_0 from the axis can be written in the form

$$\vec{W}_{\perp}^{(1)}(s) = \frac{\vec{r}_0}{a} \sum_n \frac{2k_{1n}}{(\omega_{1n}a/c)} \sin \frac{\omega_{1n}s}{c}. \quad (3.6a)$$

The k_{1n} 's are again defined in terms of the charge-free synchronous mode properties by

$$k_{1n} = \frac{[E_{zn}(r = a)]^2}{4u_n}. \quad (3.6b)$$

Here $E_{zn}(r = a)$ is the synchronous longitudinal electric field component evaluated at the disk hole radius. The dashed curve in Fig. 6(a) shows how 495 of these sine-like dipole modes add to produce the dipole wake for the SLAC structure. Again,

an analytic extension* must be added to produce a useful short-range wake.²⁴ The solid curve in Fig. 6(a) shows the total wake which results again assuming an analytic extension based on $Z_R(\omega) \sim \omega^{-3/2}$. The dot-dash curves show the wake for the lowest dipole mode, which is important in beam break-up calculations.

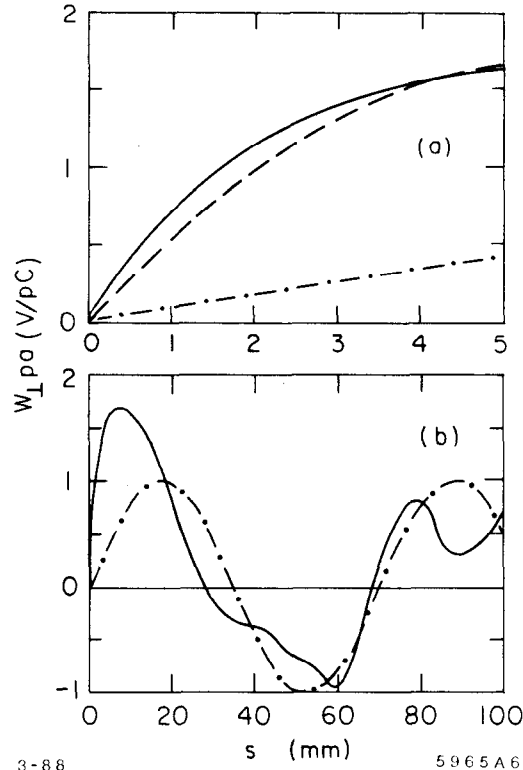


Fig. 6. Short range dipole wake for the SLAC structure. Dashed curve shows the sum of 495 modes, dot-dash curve the lowest frequency dipole mode.

Field matching across a boundary parallel to the cavity axis at the radius of the beam tube, as shown in Fig. 4(b), has also been used to obtain the field driven by a point charge passing through a single pillbox resonator with beam tubes.²⁶ In this calculation the Fourier transformed field components are used, and therefore the impedance (in this case the longitudinal impedance), rather than the wake potential, is the more direct result of the calculation. As opposed to the case for KN7C and TRANSVERS where the charge-driven wake is obtained by summing solutions to the source-free Maxwell's equations, the boundary problem here is solved directly for the source-driven fields. More recently Henke²⁷ has extended

* It should be noted that, for both the monopole and dipole cases, the optical resonator model predicts a more complicated form for $Z_R(\omega)$ unless ω_N is on the order of $2\pi cd/a^2$ or larger, where d is the periodic length and a is the beam hole radius.

this work to case of a finite chain of identical pillbox cells. He shows how the impedance of a single cell is gradually perturbed, as the number of cells increases, until it approaches a synchronous delta-function resonance for an infinite periodic structure. He also finds, for a single pillbox resonator with a large outer radius, that $Z_R(\omega)$ falls off at high frequencies as $\omega^{-1/2}$, in agreement with the result of the diffraction model to be discussed in Sec. (3.5).

Finally, under the heading of field matching techniques, we should mention several papers in which the longitudinal and transverse impedances are calculated for simple cylindrically symmetric structures with right angle jumps in cross section.^{28,29} These structures represent either pillbox cavities of arbitrary diameter in which the incoming and outgoing beam tubes can be different in radius, or collimators between equal or unequal beam tubes. Thus the field matching must be carried out at discontinuity planes normal to the axis, as shown in Figs. 4(c) and (d). As in the previous calculation, the field expansions are carried out using Fourier-transformed field components. This again gives an impedance rather than a wake potential as the direct result of the calculation. According to the theorem of conservation of difficulty, it requires more expansion coefficients to calculate the impedance at high frequencies, while more mesh points are required to compute the time domain wake potential at short distances. Thus, the two are equally difficult to obtain. However, in the case of a collimator between equal beam tubes, it can be shown²⁸ that the longitudinal impedance approaches a constant. This leads to an analytic expression for the loss parameter for a short Gaussian bunch,

$$k_\ell = \frac{Z_0 c \ln(a/b)}{\pi^{3/2} \sigma_z} , \quad (3.7)$$

where a is the radius of the beam pipe and b is the radius of the hole in the collimator.

3.4 Wake Potentials for Closed Cavities: The Condon Method

In 1941 E. U. Condon³⁰ introduced a technique for calculating the fields produced by currents and charges passing through a closed cavity. In the so-called Condon method, the vector and scalar potentials for the charge-driven fields are expanded in terms of the potentials for the normal modes of the charge-free cavity using the Coulomb gauge. Relatively simple expressions for the time-dependent expansion coefficients can be written in terms of the time-varying charge and current distributions which describe a point charge passing across the cavity.

Using the Condon method, Chao and Morton³¹ calculated the fields produced by a point charge moving at $v = c$ through the simplest possible cavity: two parallel conducting planes a distance g apart, with the charge moving on a path normal to the planes. They showed that the fields sketched in Fig. 2(f), which seem intuitively reasonable, are in fact rigorously correct. Assuming a test charge

following at distance s behind a unit driving charge, K. Bane³² integrated the longitudinal electric field in Ref. 31 to obtain the longitudinal wake potential:

$$2\pi\epsilon_0 W_z(s) = 2\delta(s) \ln \left[\frac{g}{s} \right] - 2 \sum_{n=1}^{\infty} \delta(2ng - s) \ln \left[\frac{s^2}{(s+g)(s-g)} \right] - \frac{1}{g} \left\{ \frac{1}{\left[\frac{s}{2g} \right]_{IP} + \frac{s}{2g}} - \frac{1}{\left[\frac{s}{2g} \right]_{IP} + \frac{s}{2g} + 1} \right\} \quad (3.8a)$$

Here IP denotes the integer part. Equation (3.8a) is plotted in Fig. 7. This wake is important because it is one of the few cases, if not the only case, for which an exact analytic expression has been obtained for the time domain wake for a physical structure of interest.

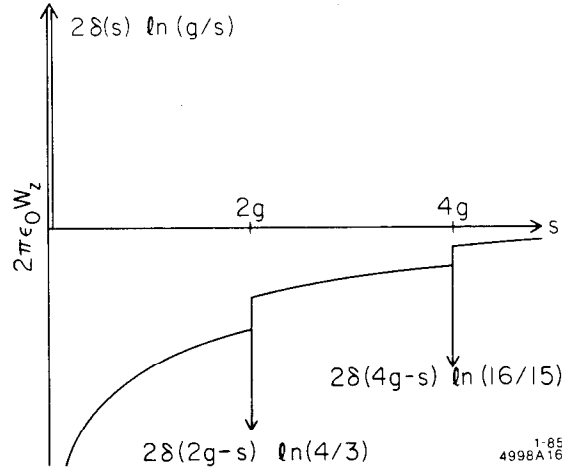


Fig. 7. Longitudinal wake potential for a point charge moving perpendicular to two parallel metallic planes.

Note that, although the geometry of the structure generating the wake is extremely simple, the wake potential function is rather complex and is replete with delta functions. The wake potential is everywhere accelerating except at $s = 0$. The driving charge itself experiences an infinite retarding potential at the moment it exits through the second plane. Spherical wavefronts, which expand with the velocity of light, are generated when the charge enters through the first plane and again when it leaves through the second plane. On the axis two of these wavefronts join in the double cusp geometry shown at position X in Fig. 4(f). When a trailing particle meets and passes through this singularity or a later reflection of it, it will experience a finite accelerating potential given by the third term on the right hand side of Eq. (3.8a). For small s this accelerating potential diverges as $1/s$. If

s happens to be a multiple of $2g$, the test particle will travel with the singularity across the cavity and will experience an infinite accelerating potential.

Using causality, the wake potential for two parallel plates should be the same as the wake potential for a closed pillbox cavity if $s < s_0 \equiv (4b^2 + g^2)^{1/2} - g$, where b is the radius of the pillbox and g its length. That is, no signal can propagate from the point where the driving charge enters the cavity, be reflected from the outer wall, and return to the path followed by the driving charge within a distance s_0 behind it. The wake potential can be written in terms of the normal modes of the cavity following the form of Eq. (3.3),

$$\pi \epsilon_0 g W_z(s) = 4 \sum_{n=1}^{\infty} \sum_{p=0}^{\infty} \epsilon_p \frac{1 - (-1)^p \cos\left(\frac{\omega_{np}g}{c}\right)}{j_n^2 J_1^2(j_n)} \cos\left(\frac{\omega_{np}s}{c}\right). \quad (3.8b)$$

Here, $\epsilon_p = 1/2$ for $p = 0$, $\epsilon_p = 1$ for $p \neq 0$ and j_n is the n^{th} root of J_0 . In Ref. 2, Sec. 3.3, the preceding two expressions for the longitudinal wake potential, which should agree for $s < s_0$, are compared. It is found that the sum in Eq. (3.8b) does not produce a smooth function, but a function which instead oscillates rapidly about an average value given by Eq. (3.8a). The period of the oscillation decreases as the number of terms in the sum in Eq. (3.8b) is increased. By extrapolation, the function will oscillate infinitely fast as the number of terms in the sum becomes infinite. Thus, both the value and the slope of the resulting function are undefined at every point. However, a convolution of this ill-behaved Green's function with a smooth bunch distribution will produce a well-behaved bunch potential.

In Ref. 3 the Condon method is applied to derive the wake potential for a closed cavity of arbitrary shape. Assume a driving charge and a test charge which both move at velocity $v = c$ on paths parallel to the z axis in a cavity with highly conducting walls. Let the driving and test charges be at transverse distances \vec{r}_0 and \vec{r} , respectively from the z axis. The driving charge crosses the cavity from $z = 0$ to $z = L$, while the test charge passes along a path from $z = z_1$, to $z = z_2$. For certain special cavity geometries it can now be shown^{3,33} that the wake potentials per unit length in Eqs. (2.2) can be written in the form

$$W_z(\vec{r}_0, \vec{r}, s) = 2H(s) \sum_n k_{nz}(\vec{r}_0, \vec{r}) \cos \frac{\omega_n s}{c}, \quad (3.9a)$$

$$\vec{W}_{\perp}(\vec{r}_0, \vec{r}, s) = 2H(s) \sum_n \vec{k}_{n\perp}(\vec{r}_0, \vec{r}) \sin \frac{\omega_n s}{c}, \quad (3.9b)$$

where

$$H(s) = \begin{cases} 0 & s < 0 \\ 1/2 & s = 0 \\ 1 & s > 0 \end{cases}$$

and

$$k_{nz}(\vec{r}_0, \vec{r}) = \frac{V_n^*(\vec{r}_0) V_n(\vec{r})}{4u_n}, \quad (3.10a)$$

$$\vec{k}_{n\perp}(\vec{r}_0, \vec{r}) = \frac{V_n^*(\vec{r}_0) \vec{\nabla}_\perp V_n(\vec{r})}{4u_n \frac{\omega_n}{c}}. \quad (3.10b)$$

Here, $V_n(\vec{r})$ is the voltage that would be gained by a nonperturbing test particle crossing the cavity in which u_n is the stored energy in the n^{th} mode. Assuming fields varying as $\exp(i\omega t)$, then

$$V_n(\vec{r}) = \int_{z_1}^{z_2} E_{zn}(\vec{r}, z) \exp\left(\frac{i\omega z}{c}\right) dz, \quad (3.11)$$

with a similar expression for $V_n(\vec{r}_0)$. Table I gives a summary of the cavity geometries in which the wake potentials are given by Eqs. (3.9). Note that the longitudinal and transverse wake potential are related by the Panofsky–Wenzel theorem, Eq. (2.20):

$$\frac{\partial \vec{W}_\perp}{\partial s} = \vec{\nabla}_\perp W_z.$$

Although the preceding relations, Eqs. (3.9), are strictly valid only for particles with $v = c$, the wake potential concept is useful for high energy particles with $v \approx c$. It can be shown³³ that the correction terms to the wake potentials are then proportional to γ^{-2} .

The wake potentials for a cylindrically symmetric periodic structure are of particular importance. Equations (2.17) give the radial dependence of the wake potential for this case, and the function $F(s)$ is fixed by Eqs. (3.9). The multipole wake potentials can now be written

$$W_z^{(m)} = 2 \left(\frac{r_0}{a}\right)^m \left(\frac{r}{a}\right)^m \cos m\theta \sum_n k_n^{(m)}(a) \cos \frac{\omega_n^{(m)} s}{c}, \quad (3.12a)$$

$$\vec{W}_\perp^{(m)} = 2m \left(\frac{r_0}{a}\right)^m \left(\frac{r}{a}\right)^{m-1} \left[\hat{r} \cos m\theta - \hat{\theta} \sin m\theta \right] \sum_n \frac{k_n^{(m)}(a)}{\omega_n^{(m)} a/c} \sin \frac{\omega_n^{(m)} s}{c} \quad (3.12b)$$

The driving charge is assumed to be at $\theta = 0$, a is the radius of the beam aperture region and

$$k_n^{(m)}(a) = \frac{\left[E_{zn}^{(m)}(r = a) \right]^2}{4u_n^{(m)}}, \quad (3.13)$$

where $u_n^{(m)}$ is the stored energy per unit length in the n^{th} mode with azimuthal symmetry $e^{im\theta}$.

Table ICases for which Eqs. (3.9a) and (3.9b) give the wake potentials in the limit $v \approx c$.

Case	Eq. (3.9a) Valid for W_z	Eq. (3.9b) Valid for \mathbf{W}_\perp
(a) Test charge and driving charge follow different paths in a closed cavity of arbitrary shape.	No	No
(b) Test charge and driving charge follow the same path in cavity of arbitrary shape.	Yes	No
(c) Velocity \vec{v} is in the direction of symmetry of a right cylinder of arbitrary cross section.	Yes	Yes
(d) Both driving charge and test charge move in the beam tube region of an infinite repeating structure of arbitrary cross section.	Yes	Yes
(e) Both particles move near the axis of any cylindrically symmetric cavity.	Yes	Yes

The most important longitudinal wake potential is that for the azimuthally symmetric $m = 0$ modes. If all the dimensions of a structure or cavity are changed by a scale factor ζ , the frequencies of the n^{th} mode will vary as $\omega_n \sim \zeta^{-2}$ and the u_n 's for a given E_{zn} will vary as ζ^2 . From Eq. (3.13) the loss parameters will therefore vary as $k_n \sim \zeta^{-2} \sim \omega_n^2$. Thus, for $m = 0$ the longitudinal wake potential per unit length at a distance $s \sim \zeta \sim \omega_n^{-1}$ behind the driving charge will also vary as $W_z^{(0)} \sim \zeta^{-2} \sim \omega_n^2$. This is true both for the wake potentials for each mode and for the total wake. The scaling as a function of beam aperture, if the other structure dimensions and the distance s are kept fixed, is less clean. A simple model in which the energy in the electric field is stored mainly in the beam hole region suggests that the k_n 's should vary as a^{-2} . Since the ω_n 's are only weakly dependent on the beam aperture, the short range longitudinal wake should also vary as a^{-2} . However, the diffraction model (next section) predicts that $W_z^{(0)} \sim a^{-1}$. Computer calculations for the SLAC structure, using an analytic extension based on the optical resonator model, give $W_z^{(0)} \sim a^{-1.68}$.

The most important transverse wake potential is the dipole wake, given by Eq. (3.6a). For a structure with all dimensions scaled by a factor ζ , the wake

potential per unit length for a fixed driving charge offset will vary as $W_{\perp}^{(1)}(s\zeta) \sim \zeta^{-3} \sim \omega_n^3$. If the aperture a is varied while s and the periodic length are kept fixed, then Eq. (3.6a) predicts $W_{\perp}^{(1)}(s) \sim a^{-4}$ for small s , again assuming the k_n 's vary as a^{-2} . The diffraction model (Sec. 3.5), however, predicts $W_{\perp}^{(1)} \sim a^{-3}$. Numerical calculations on the SLAC structure tend to agree with the a^{-3} dependence for $s \ll a$. The longitudinal wake associated with the dipole mode is

$$W_z^{(1)} = -\frac{2r_0 r}{a^2} \cos \theta \sum_n k_n^{(1)}(a) \cos \frac{\omega_n^{(1)} s}{c}. \quad (3.14)$$

This wake scales as $W_z^{(1)}(s\zeta) \sim \omega_n^4$ for fixed driving charge and field point offsets.

3.5 The Diffraction Model

As discussed previously, the wake potential at very short distances behind a driving point charge cannot be obtained from a sum of modes for a closed cavity or infinite periodic structure because of the unacceptable computation time. In a time domain program such as TBCI, a small Gaussian bunch with $\sigma_z \sim \epsilon/4$ must be used to obtain a short-range wake which is accurate at distance $s \approx \epsilon$. Even using a "moving window,"³⁴ which discards the long-range wake as the calculation proceeds, requires a computation time which varies as ϵ^{-2} . Some problems, such as an obstacle (e.g., single iris) in a waveguide, must be approached from the beginning as a scattering problem using a continuous spectrum of traveling waves rather than discrete modes. To calculate the impedance at higher frequencies (and hence the wake potential at shorter distances), the number of coefficients in the field matching expressions must be increased and again the computation time will increase as least as fast as ϵ^{-2} .

For the case of a wake potential obtained from a sum of modes, an analytic extension, Eq. (3.5), was used to approximate the wake from the uncalculated modes. This expression is based on the so-called optical resonator mode²³ in which the diffraction loss from the electromagnetic fields in an optical resonator formed by two circular disks is compared, using Babinet's principle, to the diffraction loss for the plane-wave-like field of a point charge moving on the axis of an infinite array of thin conducting sheets with circular holes. This give an impedance which falls off at high frequency as $Z_R(\omega) = A\omega^{-3/2}$ and a short-range wake which approaches a constant as $s \rightarrow 0$. Using Eq. (2.15a) and treating the bunch current distribution as constant up to frequency c/σ , the loss factor becomes for $\sigma \rightarrow 0$

$$k_{\ell} \approx k_{\ell}(\text{modes}) + \frac{2A}{\pi\omega_N^{1/2}} \left[1 - \frac{(\sigma\omega_N)^{1/2}}{c} \right], \quad (3.15a)$$

where ω_N is the highest frequency in the model sum. The constant A in this expressing and in Eq. (3.5) can be expressed in terms of the structure parameters

using the optical resonator model. Per unit length of structure, it can be written²³

$$A = \frac{\pi B C_{SV} \omega_{SV}^{3/2}}{2d}, \quad (3.15b)$$

where d is the period length, g is the cell gap length, $C_{SV} = 650$ ohms is the ‘‘Sessler–Vainshtein’’ constant, and ω_{SV} is the Sessler–Vainshtein frequency

$$\omega_{SV} \equiv \frac{c\sqrt{gd}}{4a^2}.$$

The constant B is a slowly varying ‘‘fudge factor’’ which approaches unity for $(\omega_N/\omega_{SV}) \rightarrow \infty$. For 450 modes in the SLAC structure, $\omega_N/\omega_{SV} \approx 30$ and $B \approx 0.6$. If the ratio ω_N/ω_{SV} is significantly less than thirty or so, the $\omega^{-3/2}$ impedance variation is no longer valid and a more complicated impedance function calculated from the optical resonator model must be used.²³

As mentioned previously, the applicability of the optical resonator model to the calculation of the loss in a periodic structure of finite length is questionable. For example, Balakin and Novokhatsky³⁵ find a loss parameter for a periodic structure a few cell’s in length which varies as $\sigma^{-1/2}$ for short bunches, implying a high frequency impedance which varies as $\omega^{-1/2}$. On the other hand, R. Palmer³⁶ argues for a loss parameter per unit length for such a structure which approaches a constant, implying $Z_R(\omega) \sim \omega^{-\alpha}$ where α is greater than one.

Before resolving these apparent inconsistencies in the next section, we consider the wake potentials and loss parameter for a short bunch passing through a single cavity. Application of a diffraction model to a single pillbox cavity with beam tubes was originally suggested by Lawson,³⁷ and has recently been investigated in detail by Bane and Sands.⁴ They find that the real part of the high frequency impedance is

$$Z_R(\omega) = \frac{Z_0}{2\pi^{3/2}} \sqrt{\frac{cg}{a^2\omega}} = A\omega^{-1/2}, \quad (3.16a)$$

where a is the pipe radius and g the axial length of the cavity. An analytic extension to the longitudinal wake potential can be obtained for this case, using Eq. (2.14),

$$\Delta W_z(s) = \frac{Z_0 c}{\pi^2 a} \sqrt{\frac{g}{2s}} \left[1 - 2C \left(\sqrt{\frac{2\omega_N s}{\pi c}} \right) \right], \quad (3.16b)$$

where C is the Fresnel cosine integral and ω_N is again the upper frequency limit of the sum over modes. This function, of course, diverges as s approaches zero. The total loss factor can be divide into that part due to the trapped modes in the cavity, $\omega_n \lesssim \omega_c$ where $\omega_c = 2.4c/a$ is the cutoff frequency for the beam tube, and

a part due to diffraction, $\omega \geq \omega_c$. For very short bunches, the diffraction loss per cell can be obtained by substituting Eq. (3.16b) in Eq. (2.15a) and assuming the bunch spectrum is flat to frequency $\omega = c/\sigma$ and zero beyond. The result is

$$[k_\ell(\sigma)]_{\text{Diff}} = \frac{Z_0 c}{\pi^{5/2} a} \sqrt{\frac{g}{\sigma}} \left[1 - \left(\frac{\omega_c \sigma}{c} \right)^{1/2} \right]. \quad (3.17)$$

An exact calculation⁴ using a gaussian spectral distribution $e^{-\omega^2 \sigma^2 / c^2}$ instead of the simple rectangular distribution gives the same result except that the constant 1 inside the bracket is replaced $\Gamma(1/4)/4 = 0.908$.

The dipole wake potential in the diffraction limit is also of interest. Bane and Sands⁴ obtain this as

$$[W_\perp(s)]_{\text{Diff}} = \frac{2^{3/2} Z_0 c}{\pi^2 a^3} \sqrt{g s}. \quad (3.18)$$

The transverse impulse factor, Eq. (2.5), becomes⁴ for a gaussian bunch,

$$[k_\perp(\sigma)]_{\text{Diff}} = (4.36..) \frac{Z_0 c}{\pi^3 a^3} \sqrt{g \sigma}. \quad (3.19)$$

3.6 Transition Between a Single Cavity and a Periodic Structure

In a series of recent papers and reports, the longstanding controversy over the high frequency behavior of the impedance for a periodic structure has been resolved. A definitive calculation by Heifets and Kheifets³⁸ shows that $Z(\omega) \sim \omega^{-1/2}$ if

$$\omega \gg \frac{c M d}{a^2}, \quad (3.20a)$$

where M is the number of cells in the structure (assumed to be large), d is the period and a is the iris radius. Thus the wake potential and loss factor follow Eqs. (3.16) and (3.17) if

$$\sigma \approx \frac{c}{\omega} \ll \frac{a^2}{M d}. \quad (3.20b)$$

On the other hand, the high frequency impedance will vary as $Z(\omega) \sim \omega^{-3/2}$ if³⁸

$$\omega \ll \frac{c M^{2/3} d}{a^2}, \quad (3.21a)$$

and we are in the diffraction regime, $\omega \gg cd/a^2$. We assume also that the disks in the periodic structure are relatively thin so that $d \approx g$. In terms of the bunch

length, Eq. (3.21a) implies

$$\frac{a^2}{d} \gg \sigma \gg \frac{a^2}{M^{2/3}d}. \quad (3.21b)$$

For the SLAC structure parameters ($M = 85$, $a = 1.165$ cm, $d = 3.5$ cm), Eqs. (3.20b) and (3.21b) give the regime where neither scaling is valid:

$$0.05 \text{ mm} < \sigma < 0.2 \text{ mm}. \quad (3.22)$$

Thus for $\sigma \lesssim 0.05$ mm, the impedance and loss parameters follow Eqs. (3.16a) and (3.17). For $\sigma \gtrsim 0.2$ mm, the standard expressions based on the optical resonator model should be valid.

The relation

$$\omega_t \approx \frac{cMd}{a^2},$$

for the transition between the $Z(\omega) \sim \omega^{-1/2}$ and $Z(\omega) \sim \omega^{-3/2}$ impedance regimes has also been obtained by Gluckstern³⁹ and by Palmer.⁴⁰ The note by Palmer gives a clear picture in simple physical terms of diffraction in a multi-cavity structure and the physical basis for the transition between the two regimes.

4. SOME APPLICATIONS OF WAKE POTENTIALS

4.1 Single Bunch Beam Loading and Energy Spread

A single bunch passing through a cavity will lose energy to all modes with a longitudinal electric field up to a frequency $\omega \sim 1/\sigma$. The interaction of a bunch with an externally driven accelerating mode must be treated by superposition. The energy loss to higher modes will be predominately to the cylindrically symmetric $m = 0$ modes for particles near the structure axis. To show this, we first make the reasonable guess that the loss parameters per mode for the dipole and monopole modes are on the average roughly equal at comparable frequencies. There are, however, twice as many dipole modes per unit frequency interval as monopole modes.²⁴ Since $E_z \sim r$ for the dipole mode, the ratio of the loss to dipole modes compared to monopole modes will be

$$\frac{\delta U(m=1)}{\delta U(m=0)} \approx 2 \left\langle \left(\frac{x}{a} \right)^2 \right\rangle. \quad (4.1)$$

For example, for an orbit with an rms excursion of 1 mm in the SLAC structure ($a \approx 1$ cm), the above ratio is 2%. Thus losses to dipole and higher multipole mode can in general be neglected.

For a single gaussian bunch, the loss to each mode is weighted by the gaussian form factor in Eq. (2.10c). The ratio of loss to all modes compared to the loss to the fundamental mode ($n = 0$) only is then

$$B(\sigma) = \frac{1}{k_0} \sum_{n=0}^{\infty} k_n e^{-\omega_n^2 \sigma^2 / c^2}. \quad (4.2)$$

Here B is called the beam loading enhancement factor, and we have assumed $\omega_0 \sigma / c \ll 1$ for the fundamental accelerating mode. A plot of B for the SLAC structure is shown in Fig. 8. The solid curve shows $B(\sigma)$ using the standard analytic extension assuming $Z_R(\omega) \sim \omega^{-3/2}$. The dashed curve gives an estimate in which k_ℓ is taken to be one-half that given by Eq. (3.17) for $\sigma \rightarrow 0$, in agreement with recent TBCI simulations by K. Bane.⁴¹ However, according to Eq. (3.23) the transition to the $\sigma^{-1/2}$ variation in k_ℓ should not take place until very short bunch lengths, less than 0.05 mm, have been reached. It is not yet understood why time domain mesh calculations seem to show a transition to a $\sigma^{-1/2}$ behavior at longer bunch lengths than might be expected (see also Ref. 35).

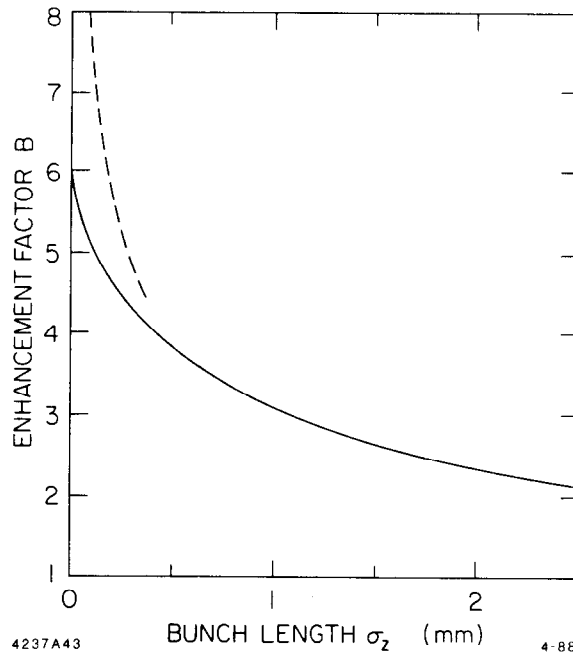


Fig. 8. Beam loading enhancement factor as a function of bunch length for the SLAC structure. Dashed curve shows the asymptotic behavior of the enhancement factor given by recent TBCI calculations.⁴¹

The energy spread within a single bunch is of great interest for linear colliders and for linacs for FEL's. In general, the energy variation within the bunch will be the superposition of the sinusoidal rf accelerating potential and the bunch potential given by Eq. (2.3a). As is well known, this energy spread can be reduced by running the bunch off the crest of the accelerating wave, such that the slope of the accelerating wave tends to cancel the average slope of the beam induced potential. In Ref. 2., Sec. 12.3, the full energy spread (containing 90% of the total charge) is plotted as a function of bunch charge for several bunch lengths for the SLAC accelerating structure, at the off-crest phase angle which minimize this energy spread. The resulting minimum spread is clearly divided into two regimes. At low bunch charge, the spread is dominated by the curvature of the rf wave near the wave nest and is given by

$$\left(\frac{\Delta V}{V_0}\right)_{90\%} \approx 50 \left(\frac{\sigma_z}{\lambda_0}\right)^2 \quad (4.3a)$$

At large values of bunch charge, the energy spread is dominated by the bunch wake, and is given roughly by

$$\left(\frac{\Delta V}{V}\right)_{90\%} \approx 0.3 \frac{\eta_b}{\cos^2 \theta} \quad (4.3b)$$

Here η_b is the efficiency for the extraction of energy from the accelerating mode given by

$$\eta_b = \frac{Gq \cos \theta}{u} = \frac{4k_0q \cos \theta}{G} \quad (4.4)$$

where G is the peak accelerating gradient, θ is the off-crest phase angle and k_0 is the loss parameter for the accelerating mode per unit length. Equations (4.3) are quite crude, especially in the transition region where the two energy spreads are comparable. The minimum full-width spread in this region tends to be somewhat lower than either expression would indicate.

Equations (4.3b) and (4.4) imply that the energy spread scales as

$$\frac{\Delta V}{V} \sim \frac{N}{G\lambda^2} \quad (4.5)$$

where N is the number of particles per bunch, for a given accelerating structure geometry.

Based on the diffraction model in the short bunch regime, K. Bane⁴¹ has also calculated the rms energy spread remaining after the linear part of the wake has

been cancelled by the slope of the rf wave. His result can be written

$$\sigma_\epsilon = 0.214 q k_{tot} , \quad (4.6)$$

where $k_{tot} = Bk_0$ is the total loss parameter, given by Eq. (3.17) for very short bunches. Combining this expression with Eq. (4.4),

$$\frac{\sigma_\epsilon}{\bar{G}} \approx .054 \frac{B\eta_b}{\cos^2 \theta} , \quad (4.7)$$

where $\bar{G} = G \cos \theta$ is the effective accelerating gradient. The required off-crest angle in the short bunch limit is, using the linear wake for a gaussian bunch obtained from Ref. 4,

$$\sin \theta \cos \theta \approx .014 \frac{B\eta_b}{\sigma_z/\lambda_0} . \quad (4.8)$$

To Eq. (4.7) must be added the energy spread due to the curvature of the rf wave,

$$\frac{\sigma_\epsilon}{\bar{G}} \approx 20 \left(\frac{\sigma_z}{\lambda} \right)^2 . \quad (4.9)$$

A somewhat different approach to the problem of estimating the single bunch energy spread for short bunches is given by R. Palmer,⁴² who uses a four-particle model to simulate the bunch.

Sometimes the actual functional form for the single bunch energy spectrum may be required. If the total energy eV at time t is the superposition of the rf wave and the single bunch wake potential, then using $I(t) = dN/dt$ the particle distribution as a function of energy eV is

$$\frac{dN}{dV} = \frac{I[f^{-1}(V)]}{V'[f^{-1}(V)]} , \quad (4.10)$$

where $V'(t) = dV/dt$ and $t = f^{-1}(V)$. A quantitative comparison between the measured and calculated energy spectrum for a single bunch in the SLAC accelerator is given in Ref. 43.

4.2 Single Bunch Transverse Dynamics

It is often useful to model the essentially continuous charge distribution in a real electron bunch by a limited number of macroparticles. A simple but very useful model is based on just two particles, a head and a tail particle located nominally at $\pm\sigma_z$ with respect to the bunch center. In the absence of transverse wakefields, the two particles independently undergo transverse oscillations having betatron wavelengths determined by the strength of the focussing lattice and

the energy of the particle. Suppose now that the transverse wake potential is turned on, and that the two particles have exactly the same energy and betatron wavelengths. The lead particle will continue to undergo transverse oscillations as before, but the tail particle now behaves like a harmonic oscillator driven on resonance. If accelerating gradient is ignored, the amplitude of the transverse motion of the tail particle will increase linearly with distance z according to

$$\frac{\Delta x}{x_0} = \frac{eq W_{\perp}(2\sigma_z) z}{4E_0 k_{\beta}} \quad , \quad (4.11)$$

where x_0 is the initial amplitude (assumed to be the same as the amplitude of the lead particle), E_0 is the particle energy and $k_{\beta} = 2\pi/\lambda_{\beta} \sim E_0^{-1}$. If the transverse delta-function dipole wake potential as shown in Fig. 6 is approximated by $W_{\perp}(s) = W'_{\perp}s$ for small s , then

$$W_{\perp}(2\sigma_z) \approx 2\sigma_z W'_{\perp} \quad . \quad (4.12)$$

Per unit length of a SLAC-type structure ($a/\lambda = 0.11$) operating at wavelength λ ,

$$W'_{\perp} \approx \frac{2.4 \times 10^{14}}{[\lambda(m)]^4} \frac{V}{C - m^3} \quad . \quad (4.13)$$

This scales^{2,41} with beam aperture for a fixed operating wavelength in the regime where the optical resonator model is valid approximately as $a^{-3.5}$. As discussed previously, Eq. (3.18) must be used for extremely short bunches such that the single-cell diffraction wake is dominant. In this case the wake has a $s^{1/2}$ dependence and therefore as $s \rightarrow 0$ the slope becomes infinite.

The linear growth with distance in the amplitude of the oscillation of the tail particle, as given by Eq. (4.11), can be suppressed by introducing an energy difference between the lead and the tail particles. The tail particle then acts like a harmonic oscillator driven off resonance. This suppression, called BNS damping (for Balakin, Novokhatsky and Smirnov, who first introduced the concept), is essentially complete if the energy difference, $E_{\text{head}} - E_{\text{tail}}$, is chosen to be

$$\Delta E = \frac{eq W_{\perp}(2\sigma_z)}{4k_{\beta}^2} \quad , \quad (4.14)$$

A review of the two-particle model, its extension to N particles, and the application of BNS damping to a continuous charge distribution in a realistic accelerator (the SLC at SLAC) is given by K. Bane.⁴⁴

Assuming that the transverse emittance growth due to linac wakefields has been suppressed by BNS damping, other transverse effects can then be troublesome. As an example, the transverse positions of the focussing quadrupoles

will jitter due to ground motion. This seismic noise, arising from both natural and manmade causes, gives small random transverse kicks to the bunch at each quadrupole. As a result, the transverse bunch displacement undergoes a random walk growth along the linac. If the final displacement of the bunch is comparable to the transverse bunch dimension, there will be a loss in luminosity in a linear collider. This and other transverse single bunch beam dynamics effects are treated by R. Ruth.⁴⁵

4.3 Multiple Bunch Wakefield Effects

In a conventional pulsed accelerator, a beam pulse is accelerated which is typically several structure filling times in length, and sometimes much more. The number of rf cycles in one filling time for a critically coupled standing wave structure, or for a traveling wave structure with attenuation parameter $\tau = 0.5$, is $n_f = Q_0/2\pi$. For the SLAC structure this gives $n_f \approx 2 \times 10^3$, while for a typical linear collider structure at higher frequency and lower τ , $n_f \approx 500$. This is the time a cavity or structure can “remember” the longitudinal wakefields due to the passage of a single bunch. If bunches are located one rf wavelength apart, the fundamental mode wake potentials for n_f bunches will add nearly linearly to produce the steady state beam loading voltage. The wakes for higher modes will be incoherent from bunch to bunch and will therefore be suppressed by a factor on the order of $n_f^{1/2}$ with respect to the fundamental mode. Thus for steady state operation the energy spread produced by higher modes will be a few percent of the beam loading voltage.

In a linear collider, however, it is contemplated that a relatively short train of $N_b = 10$ or 20 bunches, spaced apart by a few wavelengths at the fundamental mode, will be employed. By injecting the bunch train into a traveling wave structure before the structure is completely filled with rf, it can be shown⁴⁶ that the energy difference between bunches due to fundamental mode beam loading can be compensated to the order of 2×10^{-3} , while still extracting about 1% per bunch of the energy in the fundamental mode, giving a total energy extraction efficiency of 10-20%. Without this compensation, the energy of the last bunch would be $N_b\eta_b/2 \approx 5-10\%$ lower than that of the first bunch. Higher order longitudinal modes, however, will also contribute to the bunch to bunch energy spread. This contribution can be estimated from the long range longitudinal wake potential, given for the SLAC structure in Fig. 9. The dots shows bunch locations at integer multiples of the fundamental mode wavelength. It is seen that higher modes would contribute an rms energy spread which is about ± 0.3 times that due to the fundamental mode wake. If these energy differences added randomly for 20 bunches, the relative energy error for the last bunch would be about $0.3\sqrt{N_b}\eta_b/2 = 0.7\eta_b$, or about 10^{-2} in a typical case. To reduce this spread, two things can be done. First, larger beam aperture, relative to the SLAC design, are being considered for linear colliders. This is found to suppress the contribution

from higher modes relative to the fundamental mode by a factor of two or so. Second, new accelerating structures are being developed⁴⁷ with coupling slots for suppressing higher modes to give effective Q 's on the order of fifty or less. Thus, the higher mode wakes attenuate in a distance of two or three bunch spacing at the most. This further reduce the relative energy error by another factor three or so, giving a final relative energy spread on the order of $\pm 0.1 \eta_b$.

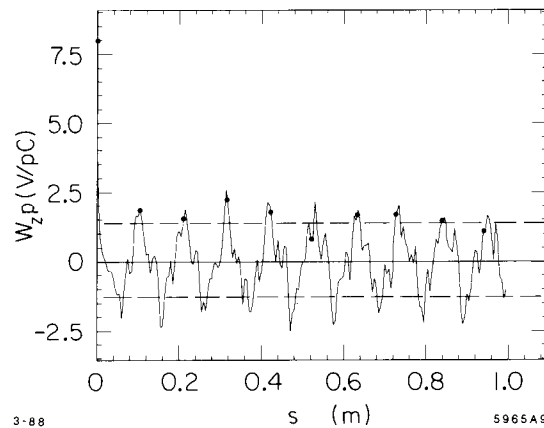


Fig. 9. Long range longitudinal wake potential per cell for the SLAC structure. Dots are spaced one wavelength apart for the accelerating mode.

Similar considerations apply to the long range transverse wake, shown in Fig. 10. Again, the long-range wake is dominated by the lowest frequency dipole mode. By perturbing the structure design, the frequency of this mode can be adjusted so that the bunch spacing is an integer multiple of its wavelength. The bunches then fall at the zero crossings of the wake for the dominant transverse mode, and the effect of this mode on the transverse displacement of subsequent bunches (cumulative beam breakup) is greatly reduced. Again, the dipole modes can be damped by a structure design with appropriate coupling slots.⁴⁷ It can be shown⁴⁸ that these two measures are adequate to suppress multibunch beam breakup to an acceptable level for typical linear collider design parameters.

4.4 Wakefields from Scrapers and Collimators

The longitudinal loss parameter for a circular collimator was given by Eq. (3.7). But what is perhaps more important, if a low emittance bunch passes close to the edge of a collimator or scraper, the resulting transverse wake potential can cause a degradation in emittance. This problem has been investigated by Bane and Morton.⁴⁹ If the bunch length is comparable to or greater than the radius a of the collimator hole (or the half width of the aperture in a window scraper), then the transverse kick at position s in the bunch is, for each edge of

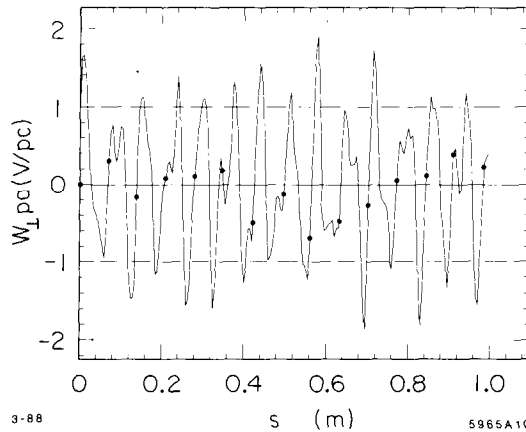


Fig. 10. Long range dipole wake potential per cell for the SLAC structure.

the scraper,

$$V_{\perp}(s) = \frac{Z_0 c \lambda(s)}{2\pi} \frac{\Delta x}{a} \quad (4.16)$$

Here, Δx is the transverse offset of the bunch from the centerline of the collimator and $\lambda(s)$ is the linear charge density. Note that the kicks received at the input and output edges of the collimator are identical, and the total kick is therefore twice that given by Eq. (4.16). For a gaussian bunch, the peak kick at the center of the bunch is⁴⁹

$$\hat{V}_{\perp}(s) = \frac{Z_0 c q}{(2\pi)^{3/2} \sigma_z} \frac{\Delta x}{a} \quad (4.17)$$

The transverse kick can be reduced by tapering the edge of the scraper. A 15° taper angle (with respect to the beam line) reduces the deflection angle, eV_{\perp}/E_0 , by a factor of two.

The loss parameters for very short bunches passing by a variety of vacuum chamber discontinuities, such as cavities and steps, are reported by Bisognano, Heifets and Yunn.⁵⁰ As an example, we take the case of a circular pipe of radius b which steps abruptly to a smaller radius a (the impedance is negligibly small for a step to a larger radius). The impedance for the inward step is (see also Ref. 51),

$$Z_0(\omega) = \frac{Z_0}{\pi} \ell n \frac{b}{a}, \quad (4.18a)$$

and the loss parameter is

$$k_{\ell} = \frac{2}{\sigma \sqrt{\pi}} \ell n \frac{b}{a}. \quad (4.18b)$$

4.5 Applications to Storage Rings

The longitudinal and transverse impedances of the vacuum chamber components in a storage ring are key ingredients in determining the threshold currents for a variety of possible instabilities. A review of basic analytic approaches to calculating these beam instabilities is given in Ref. 1. The analysis is usually carried out in the frequency domain, in terms of an impedance and a current distribution. To obtain results analytically, however, it is often necessary to make severe approximations to the form of either the impedance function or the current distribution. For more accurate quantitative results it is often desirable to turn to a time domain simulation using an ensemble of macroparticles to model the current distribution, and to then subject these particles to appropriate longitudinal and transverse kicks as determined by the time domain wake potentials. Such simulations have been particularly useful in investigating bunch lengthening effect in SPEAR,⁵² PETRA⁵³ and LEP.⁵⁴ A recent report by Nys⁵⁵ describes current work at CERN on longitudinal bunch simulations, together with a rather complete list of references to past work. Simulation of transverse single bunch stability have been developed by Siemann,⁵⁶ Brandt⁵⁷ and Nys.⁵⁸

An interesting application of the transverse wake potential to storage rings is related to the so-called fast head tail instability. This instability has been analyzed extensively in both the frequency and time domains. A time domain description using a two particle model for the bunch is, however, particularly simple.⁵⁹ We assume that the head and tail particles interchange places every half cycle of synchrotron oscillation. During the first half cycle the betatron oscillations of the head particle produce wakefields which drive the transverse oscillations of the tail particle, while during the next half cycle the roles of the particles are reversed. It is easy to show that, below a threshold current per bunch, a stable solution is possible in which the oscillation amplitudes of the two particles remain constant at a slightly reduced betatron frequency. Above the threshold current per bunch, I_b , the oscillation amplitudes begin to grow exponentially, where

$$I_b \approx \frac{16 (E_0/e) f_s}{\sum_i \overline{W}_{\perp i} \beta_i} \quad (4.19)$$

Here, $\overline{W}_{\perp i}$ is the transverse wake potential seen by the trailing particle for the i^{th} vacuum chamber component, averaged over one-half cycle of its synchrotron motion, β_i is the beta function at the component, and f_s is the synchrotron frequency. Looking at a typical short-range dipole wake as shown in Fig. 6, the average wake can be calculated if we assume that the origin is the location of the head particle and that the tail particle moves back a maximum distance $s_m \approx 2\sigma_z$ following $s = s_m \sin(\omega_s t)$. If the wake potential is now weighted by the relative

time spent at each value of s , we have

$$\overline{W}_\perp = \frac{2}{\pi} \int_0^{s_m} \frac{W_\perp(s) ds}{(s_m^2 - s^2)^{1/2}} \quad (4.20)$$

Thus, for short bunches, assuming $W_\perp(s) = W'_\perp s$, then $\overline{W}_\perp \approx (4/\pi)W'_\perp \sigma_z$. The average wake, \overline{W}_\perp , will be much less than the peak value of the wake, \widehat{W}_\perp , and the threshold current will be high. The threshold current will drop as the bunch length increases, reaching a minimum when $2\sigma_z$ is about equal to the value of $s = \hat{s}$ at the peak of the wake potential ($\hat{s} \approx a$ for a disk loaded structure), and $\overline{W}_\perp \approx 0.8\widehat{W}_\perp$. It will then slowly rise again for longer bunches. This behavior is also obtained in a frequency domain analysis⁶⁰, but the two bunch model using time domain wake potentials provides a simple picture of the underlying physics. An application of Eq. (4.19) to the PEP storage ring is given in Ref. 61.

ACKNOWLEDGMENT

I am indebted to Karl Bane for his help in generating the wake potentials shown in Figs. 5, 6, 9 and 10, and for allowing me to use some of his unpublished results on the energy spread and loss factors for short bunches in single cavities and periodic accelerating structures.

REFERENCES

1. Alexander W. Chao, AIP Conf. Proc. **105** (AIP, New York, 1983), pp. 353-523. Also SLAC-PUB-2946 (1982).
2. P. Wilson, AIP Conf. Proc. **87** (AIP, New York 1982), pp. 450-563. Also available as SLAC-PUB-2884 (1982).
3. K. Bane, T. Weiland and P. Wilson, AIP Conf. Proc. **127** (AIP, New York, 1985), pp. 875-928. Also available as SLAC-PUB-3528 (1984).
4. Karl Bane and Matthew Sands, *Wakefields of Very Short Bunches in an Accelerating Cavity*, SLAC-PUB-4441 (1987).
5. See, for example, R. Bracewell, *The Fourier Transform and its Applications*, (McGraw-Hill, New York, 1965).
6. T. Weiland, DESY M-83-02 (1983) and Nucl. Instrum. Methods **216**, 31 (1983).
7. Reference 1, Sec. 1.4.
8. W. K. H. Panofsky and W. A. Wenzel, Rev. Sci. Instrum. **27**, 967 (1956).
9. T. Weiland, Part. Accel. **15**, 245-292 (1984).

10. T. Weiland, Proceedings of the 11th Int. Conf. on High Energy Accelerators, Geneva, 1980 (Birkhäuser Verlag, Basel, 1980), pp. 570-575.
11. T. Shintake, 1984 Linear Accelerator Conf., GSI Report 84-11, Darmstadt (1984), pp. 411-413.
12. A. V. Novokhatsky, Preprint 82-157, Inst. for Nucl. Phys., Novosibirsk (1983).
13. R. Klatt and T. Weiland, 1986 Linear Accelerator Conf., SLAC-Report-303 (1986), pp. 282-285.
14. P. L. Morton, V. K. Neil and A. M. Sessler, JAP **37**, 3875 (1966).
15. Reference 1, Secs. 1.2 and 1.3.
16. Reference 2, Sec. 6.1 and Ref. 3, Sec. 4.1.
17. M. Chatard-Moulin and A. Papiernik, IEEE Trans. Nucl. Sci. **NS-26**, 3523 (1979).
18. M. Chatard-Moulin and A. Papiernik, Nucl. Instrum. and Meth. **205**, 37 (1983).
19. R. K. Cooper, S. Krinsky and P. L. Morton, Part. Accel. **12**, 1 (1982).
20. S. Kheifets and B. Zotter, CERN/LEP-TH/85-27 (1985).
21. S. Krinsky and R. Gluckstern, IEEE Trans. Nucl. Sci. **NS-28**, 26 (1981).
22. E. Keil, Nucl. Instrum. Meth. **100**, 419 (1972).
23. D. Brandt and B. Zotter, CERN-ISR/TH/82-13 (1982).
24. K. Bane and P. Wilson, Proceedings of the 11th Int. Conf. on High Energy Accelerators, Geneva, 1980 (Birkhäuser Verlag, Basel, 1980), pp. 592-596.
25. K. Bane and M. Zotter, Proc. of the 11th Int. Conf. on High Energy Accelerators, Geneva, 1980 (Birkhäuser Verlag, Basel, 1980), pp. 581-585.
26. H. Henke, CERN-LEP-RF/85-41 (1985).
27. H. Henke, CERN-LEP-RF/87-62 (1987).
28. S. Kheifets, SLAC-PUB-4133 (1986).
29. S. Kheifets, K. L. F. Bane and H. Bizek, SLAC-PUB-4097 (1987).
30. E. U. Condon, J. Appl. Phys. **12**, 129 (1941).
31. A. W. Chao and P. L. Morton, SLAC PEP-Note-105 (1975).
32. Reference 3 and private communication.
33. K. Bane, CERN/ISR-TH/8-47 (1980).
34. K. Bane and T. Weiland, Proc. of the 12th Int. Conf. on High Energy Accelerators, Fermilab, 1983, pp. 314-316. Also available as SLAC-PUB-3173 (1983).

35. V. Balakin and A. Novokhatsky, Proceedings of the 13th Int. Conf. on High Energy Accelerators, Novosibirsk, 1986, (Novosibirsk Publishing House "Nauka", 1987). pp. 135-137.
36. R. Palmer, SLAC-PUB-4433 (1987).
37. J. Lawson, Rutherford High Energy Laboratory Report RHEL/M144 (1968).
38. S. A. Heifets and S. A. Kheifets, *High Frequency Limit of the Longitudinal Impedance of an Array of Cavities*, submitted to Phys. Rev. D. also SLAC-PUB-4625 (May 1988).
39. R. L. Gluckstern, *Longitudinal Impedance of a Periodic Structure at High Frequency*. University of Maryland (1988).
40. R. B. Palmer, *A Diffraction Analysis of Longitudinal Wakes of Short Bunches*, SLAC Internal Note AAS-44 (January 1989).
41. K. Bane, private communication.
42. R. Palmer, ECFA Workshop on New Development in Particle Acceleration Techniques, Orsay, France, 1987, CERN 87-11 (1987), pp. 80-121. Also SLAC-PUB-4295 (1987).
43. R. F. Koontz et al., IEEE Trans. Nucl. Sci. **NS-24**, No. 3, 1493 (1972). Also SLAC-PUB-1917 (1979).
44. K. Bane, AIP Conf. Proc. **153** (AIP, New York, 1987), pp. 971-1014. Also SLAC-PUB-4169 (1986).
45. R. Ruth, ECFA Workshop on New Developments in Particle Accelerator Techniques, Orsay, France, 1987; CERN 87-11 (1987), pp. 147-160. Also SLAC-PUB-4430 (1987).
46. R. D. Ruth, SLAC-PUB-4541 (1988).
47. R. Palmer, SLAC-PUB-4542 (1988).
48. K. Thompson and R. D. Ruth, SLAC-PUB-4537 (1988).
49. K. L. F. Bane and P. L. Morton, Proc. 1986 Linear Accel. Conf., SLAC-303, p. 490. Also SLAC-PUB-3983 (1986).
50. J. J. Bisognano, S. A. Heifets and B. C. Yunn, *The Loss Parameters for Very Short Bunches*, CEBAF-PR-88-005, Continuous Electron Beam Accelerator Facility, Newport News, Virginia (1988).
51. S. A. Kheifets, SLAC-PUB-4133 (1986).
52. R. Siemann, CLNS 82/524, Cornell University (1982).
53. T. Weiland, DESY 81-088 (1981).
54. D. Brandt, CERN/ISR-TH/82-09 (1982).

55. V. Nys, CERN/LEP-TH/86-34 (1986).
56. R. Siemann, CBN 82-27, Cornell University (1982); R. Siemann, Nucl. Instrum. Methods **203**, 57 (1982); R. Siemann, IEEE Trans. Nucl. Sci. **NS-30**, 2373 (1983).
57. D. Brandt, LEP-Note-512, CERN (1984).
58. V. Nys, CERN/LEP-TH/87-35 (1987).
59. See, for example, Ref. 1, Sec. 2.4 and Ref. 3, Sec. 11.2.
60. See, for example, B. Zotter, CERN/ISR-TH/82-10 (1982); also LEP-Note 402, CERN (1982).
61. P. B. Wilson and L. Rivkin, PEP-Note-374, SLAC (1982).